Mapping Energy Balance Fluxes and Root Zone Soil Moisture in the White Volta Basin using Optical Imagery

Jan M.H. Hendrickx[*a], Sung-ho Hong[a], Jan Friesen[b], Halidou Compaore[c], Nick C. van de Giesen[b], Charles Rodgers[d], Paul L.G. Vlek[d]

[a]Dept. of Earth & Environ. Science, New Mexico Tech, Socorro, USA
[b]Water Resources Section, Delft University of Technology, Delft, The Netherlands
[c]National Center for Scientific and Technological Research (CNRST), Ouagadougou, Burkina Faso
[d]Center for Development Research (ZEF), Bonn University, Bonn, Germany

ABSTRACT

Accurate information on the distribution of sensible and latent heat fluxes as well as soil moisture is critical for evaluation of background characteristics. Since these fluxes are subject to rapid changes in time and space, it is nearly impossible to determine their spatial and temporal distributions over large areas from ground measurements alone. Therefore, prediction from remote sensing images is very attractive as it enables extensive area coverage and a high repetition rate. In this study, the Surface Energy Balance Algorithm for Land as implemented at New Mexico Tech (SEBAL[NM]) is used to estimate sensible and latent heat fluxes in the White Volta Basin of Ghana, West Africa. The objectives are (i) to demonstrate a SEBAL[NM] application in a part of the world were ground measurements are very scarce and (ii) to compare evapotranspiration (ET) maps obtained from Landsat and MODIS imagery, respectively. The results of this study demonstrate that SEBAL[NM] can be applied for mapping sensible and latent heat fluxes as well as soil moisture over areas where few or no ground measurements are available using common satellite products (Landsat and MODIS).

Keywords: sensible heat flux, latent heat flux, SEBAL[NM], evapotranspiration

1. INTRODUCTION

Near-surface atmospheric and soil moisture conditions have an impact upon virtually all aspects of Army activities and are increasingly affecting its systems and operations. Atmospheric turbulence can hamper the performance of optical and infrared sensors as well as acoustic detection systems. Soil moisture conditions affect operational mobility[1], detection of landmines[2-13] and unexploded ordinance, natural material penetration/excavation, military engineering activities, blowing dust and sand, watershed responses[14-20], and flooding. Near-real time data on the spatial distribution of sensible and latent heat fluxes will help (i) to make better predictions of electro-optical signals transmissions and (ii) to better initialize micro scale models for prediction of concentrations of chemical and biological agents in realistic terrains; data on soil moisture will provide critical information on operational mobility, penetration, and performance of landmine and UXO sensors as well as greatly improve the initialization of hydrologic models for the prediction of watershed responses and flooding.

The energy fluxes at the soil surface and soil moisture strongly interact with each other. We recognize two heat fluxes that transport energy between the soil surface and the atmosphere: the sensible and the latent heat flux. The sensible heat

---

[*] hendrick@nmt.edu; phone (+1) 505 835-5892; fax (+1) 505 835-6436; http://www.ees.nmt.edu/hydro/landmine

flux consists of heat transported by air "parcels". If a dry soil surface warms up during the day as a result of incoming solar radiation, the absorbed energy is partitioned between a heat flux going into the soil by conduction and one going into the air by convection. Air parcels close to the surface warm up, expand, and start rising into the cooler air above. If a wet soil surface warms up during the day, the absorbed energy is partitioned between the soil heat flux and the latent heat flux λE (W m^{-2}), which basically is the evaporation rate. The parameter λ is the latent heat of vaporization of water (J kg^{-1}) and E is the vapor flux density (kg m^{-2} s^{-1}). The partition of net available energy at the soil surface between the sensible and latent heat fluxes depends on the soil water content of the root zone[21-23]. When soil water content is high, the latent heat flux is dominant while for dry conditions the sensible heat flux prevails. The focus of this contribution is on sensible and latent heat fluxes. Direct measurements of these fluxes is too expensive and time consuming for application at regional scale and only provide point measurements at a scale that may be considerably smaller than the estimate obtained from remote sensing methods. Moreover, it is difficult to determine the area that measurements represent, especially over heterogeneous vegetation. In this study, we use the New Mexico Tech implementation of the Surface Energy Balance Algorithm for Land (SEBAL^{NM}) for estimation of the heat fluxes since it is a cost-effective and fast method that requires few or no ground observations. Best estimates of sensible and latent heat fluxes by SEBAL^{NM} from Landsat imagery have been successfully validated by Hendrickx's research group using ground measurements in the heterogeneous riparian areas of the US southwestern states[24]. In addition, best estimates of these heat fluxes by SEBAL^{NM} from MODIS imagery have been validated in New Mexico[25]. The SEBAL method has also been used in numerous other studies to assess latent heat fluxes in Idaho, Spain, Italy, Turkey, Pakistan, India, Sri Lanka, Egypt, Niger, and China[26-35]. These applications of SEBAL have demonstrated its ability to accurately estimate daily latent heat fluxes, i.e. evapotranspiration rates, on agricultural land for all stages of crop development and growth.

The overall goal of this study is to demonstrate that important background information on the components of the energy balance and soil moisture can be obtained from optical imagery anywhere in the world without using ground measurements. For this study we have selected the challenging heterogeneous tropical environment of the White Volta Basin in Ghana. The specific objectives are (i) to test SEBAL^{NM} with Landsat and MODIS imagery in the White Volta Basin of Ghana without using any ground measurements and (ii) to compare evapotranspiration maps generated from Landsat images with spatial resolution 60 m to those generated from MODIS images with spatial resolution 1000 m.

2. SURFACE ENERGY BALANCE ALGORITHM FOR LAND (SEBAL^{NM})

SEBAL is a remote sensing flux algorithm that solves the surface energy balance on an instantaneous time scale and for every pixel of a satellite image[32-34, 36]. The method is based on the computation of surface albedo, surface temperature and vegetation index from multispectral satellite data. The surface albedo is used to calculate net short wave radiation, and surface temperature for the calculation of net long wave radiation, soil heat flux and sensible heat flux. The vegetation index governs the soil heat flux by incorporating light interception by canopies, and is used to express the aerodynamic roughness of the landscape. The latent heat flux is computed as the residue of the surface energy balance. Air humidity measurements are not needed because evaporation is computed from the latent heat flux. SEBAL has been applied for water balance estimations[30], irrigation performance assessment studies[29], and for weather prediction studies[37].

SEBAL is a physically based analytical method that evaluates the components of the energy balance and determines the ET rate as the residual

$$R_n - G - H = \lambda E \tag{1}$$

where R_n is the net incoming radiation flux density (W m^{-2}), G is the ground heat flux density (Wm^{-2}), H is the sensible heat flux density (W m^{-2}), and λE is the latent heat flux density (W m^{-2}), which basically is the ET rate. The parameter λ is the latent heat of vaporization of water (J kg^{-1}) and E is the vapor flux density (kg m^{-2} s^{-1}). Evaporation E includes both bare soil evaporation and canopy transpiration.

The main challenge in the energy balance is to determine the partitioning of the available energy ($R_n - G$) into λE and H. The net radiation R_n is estimated from the remotely sensed surface albedo, surface temperature, and solar radiation calculated using standard astronomical formulae[38]. The ground heat flux G is determined through semi-empirical

relationships with R_n, surface albedo, surface temperature, and vegetation index[32-34, 36]. The most critical factor in the physically based remote sensing algorithms is to solve the equation for the sensible heat (H)

$$H = \rho_a \, c_p \, \frac{T_{aero} - T_a}{r_{ah}} \qquad (2)$$

where ρ_a is the density of air (kg m^{-3}), c_p is the specific heat of air (J kg^{-1} K^{-1}), r_{ah} is the aerodynamic resistance to heat transfer (s m^{-1}), T_{aero} is the surface aerodynamic temperature, and T_a is the air temperature either measured at a standard screen height or the potential temperature in the mixed layer[39]. The aerodynamic resistance to heat transfer is affected by windspeed, atmospheric stability and surface roughness[23]. The apparent simplicity of Eq. [2] is deceptive since T_{aero} cannot be measured by remote sensing. Remote sensing techniques measure the radiometric surface temperature T_{rad} which is not the same as the aerodynamic temperature. The two temperatures usually differ by 1 to 5 °C. Unfortunately, an uncertainty of 1 °C in $T_{aero} - T_a$ can result in a 50 W m^{-2} uncertainty in H [22] that could be approximately equivalent to an evaporation of 2 mm per day. Although many investigators have tried to solve this problem by adjusting r_{ah} or using an additional resistance term, no generally applicable method has been developed yet[40].

SEBAL is a practical method that overcomes the problem of inferring the aerodynamic temperature from the radiometric temperature and the need for near-surface air temperature measurements by directly estimating the temperature difference between T_1 and T_2 taken at two arbitrary elevations z_1 and z_2 without explicitly solving for the absolute temperature at a given height. The temperature difference for a dry surface without evaporation is obtained from the inversion of the sensible heat transfer equation setting latent heat flux $\lambda E = 0$ so that $H = R_n - G$ [32, 33, 36]

$$T_1 - T_2 = \Delta T_a = \frac{H \, r_{ah}}{\rho_a \, c_p} \qquad (3)$$

For a wet surface all available energy $R_n - G$ is used for evaporation λE so that $H = 0$ and $\Delta T_a = 0$. Field observations have indicated that land surfaces with a high ΔT_a are associated with high radiometric temperatures and those with a low ΔT_a with low radiometric temperatures. For example, in New Mexico and Idaho moist irrigated fields have a much lower ΔT_a than dry rangelands. Field measurements in Egypt and Niger[32], China[26], USA[41], and Kenya[42] have shown that the relationship between T_{rad} and ΔT_a is linear

$$\Delta T_a = c_1 \, T_{rad} - c_2 \qquad (4)$$

where c_1 and c_2 are the linear regression coefficients valid for one particular moment (the time and date the image is taken) and landscape. By using the minimum and maximum values of ΔT_a as calculated for the coldest and warmest pixel(s), the extremes of H are used to find the regression coefficient c_1 and c_2 which will prevent outliers of H-fluxes. Thus, the empirical Eq. [4] relies on spatial differences in the radiometric surface temperature rather than absolute surface temperatures, to minimize the influence of atmospheric corrections and uncertainties in surface emissivity.

Eq. [3] has two unknowns: ΔT_a and the aerodynamic resistance to heat transfer r_{ah}, which is affected by wind speed, atmospheric stability, and surface roughness. Several algorithms take a few field measurements of wind speed and treat them as spatially constant over representative parts of the landscape[43-45]. This assumption is only valid for uniform homogeneous surfaces. For heterogeneous landscapes a wind speed near the ground surface is required for each pixel. One way to overcome this problem is to consider the wind speed spatially constant at a height of 200 m above ground level. This is a reasonable assumption since at this height the wind speed is not affected by local surface heterogeneities. The wind speed at 200 m is obtained by an upward extrapolation of a wind speed measurement at 2 or 10 m assuming a logarithmic wind profile. The wind speed at each pixel is obtained by a downward extrapolation using the surface roughness, which is determined for each pixel using an empirical relationship between surface momentum roughness z_{0m} and the Normalized Difference Vegetation Index (NDVI) or the Soil Adjusted Vegetation Index (SAVI)[46]. The end result of these calculations is the determination of values for r_{ah} and ΔT_a for each pixel which allows us to find the sensible heat flux for each pixel. After inserting R_n, G, and H into Eq. [1] the latent heat flux λE or ET rate is derived for each pixel.

Is SEBAL "old technology"? At first inspection SEBAL is quite similar to other ET estimation methods that use T_{rad} and ΔT but with one significant difference: SEBAL uses an internal auto-calibration process that eliminates the need for actual measurements of T_{rad} and/or ΔT as well as for atmospheric corrections. SEBAL is automatically calibrated for biases through the regression calibration of Eq. [4] which is based on a cold and warm pixel. Thus, the surface temperature T_{rad} is used as a distribution parameter for partitioning the sensible and latent heat flux. ΔT_a floats above the land surface as it is indexed to T_{rad} (through calibration Eq. [4]) but it does not require actual measurements on the ground or atmospheric corrections.

SEBAL yields an estimate of the instantaneous ET (mm/hour) at the time of the LandSat overpass around 11:00 am. This hourly ET rate must then be extrapolated to obtain the daily ET. The extrapolation is done using the evaporative fraction (*i.e.,* the ratio of latent heat over the sum of latent and sensible heat) which has been shown to be approximately constant during the day. Therefore, multiplication of the evaporative fraction determined by SEBAL with the total daily available energy yields the daily evapotranspiration rate.

Soil moisture conditions in the root zone can be determined from the evaporative fraction using the empirical relationship[47]:

$$S = \frac{\theta}{\theta_{sat}} = e^{\frac{\Lambda - 1}{0.42}}$$

(5)

where S is relative degree of saturation, θ is volumetric water content, and θ_s is volumetric water content at saturation. The validity of Eq. [5] has been tested in several studies[21, 47] including one in New Mexico[48].

3. STUDY AREA

The White Volta flows southward across the frontier between Burkina Faso and Ghana in the Bolgatanga area which lies between latitudes 12°00´N to 10°20´N and longitudes 0°16´W to 0°16´ E (Figure 1). The study area has a Sudanese climate, characterized by a mean annual precipitation of about 1000 mm varying between 700 mm and 1100 mm. Weather conditions change drastically over the year: average monthly temperature ranges from 26°C to 32°C, with the average minimum and maximum in the ranges 19° C to 26°C and 30°C to 39°C, respectively. The rainy season is mono-modal with the rainfall peak occurring in August. The driest months are December and January; the lowest temperatures are experienced in December, while the highest temperatures occur in March. Potential evaporation is about 250% of annual rainfall; monthly averages of relative humidity range from 16% to 95%. Climate data for the Navrongo station (close to Bolgatanga) are presented in Table 1. For a full hydrological description of the White Volta Basin we refer to Amisigo and Compaore[49, 50].

Figure 1. The dotted rectangle represents the study area.

Table 1.   Temperature, precipitation, and wind speed recorded at the Navrongo weather station (1961-2003) (Source: Navrongo Meteorological Services)

	Jan	Feb	Mar	Apr	May	Jun	Jul	Aug	Sept	Oct	Nov	Dec	Year
T (°C)	27.5	29.7	32.1	32.3	30.6	28.2	27.0	26.4	26.8	28.2	28.3	27.2	28.7
P (mm)	1	3	15	51	102	130	188	273	168	51	4	2	987
WS ms^{-1}	2.2	2.3	2.2	2.5	2.4	2.0	1.8	1.5	1.3	1.3	1.4	1.8	1.9
ETp (mm)	273	312	307	248	186	134	104	89	100	151	245	269	2423

T is average temperature; P is average precipitation; WS is wind speed; ETp is average potential evapotranspiration.

The *Harmattan* wind is an important climatic phenomenon occurring during the dry season in West Africa. Dry air flows from the NE towards the SW, originating from the high Saharan pressures or anticyclones of the Azores. This dry continental air, or boreal trade wind, is hot during the day and cold during the night. This wind is often charged with dust and is responsible for the quasi-permanent presence of dry fogs from December to March[51], with a concentration of aerosols from 15 to 20 mg cm^3. This concentration can sometimes even reach 30 to 100 mg cm^3 due to violent dusts[52], with visibility reduced to less than one kilometer. Associated with *Harmattan* are burning events that start with the dry season.

The White Volta, which crosses the southern part of the Navrongo area, generally flows in a NW to SE direction, and turns sharply West at the point where the river encounters the Gambaga scarp. It is fed by a number of tributaries which include the Tono River in the West and the Red Volta in the NE part of the study area. During the wet season the vegetation, mainly composed of grasses, is dense and luxuriant. Streams and rivers in the area are subject to sudden fluctuations in water level, suggesting that there is considerable surface run-off within their catchments during heavy rainfall. During the dry season, discharge decreases and finally ceases in March. A common feature of the flow regime in the savannah is the reduction of continuous flow to a series of disconnected pools within the channel bed, separated by dry stretches of sand and rock. Human beings as well as livestock suffer from domestic water shortage, as water supply is obtained primarily from rivers, small dams, springs and boreholes. Water deficit in the soil has also an impact on the vegetation layer, which is essentially composed of deciduous trees that loose their leaves to avoid water stress. The process is characteristic of the entire Volta basin, from the drier Sahelian to the more humid savannah zones. The conditions of spatially and temporally unbalanced distribution of available water pose a challenge to the management of water resources for regional development. Hundreds of small dams have been constructed in Ghana to overcome water shortage in the dry season. The Tono Dam near Navrongo is the main reservoir providing irrigation water throughout the year, while small dams and groundwater from bore holes are used mainly as drinking water and to irrigate garden vegetables during the dry season.

The geology of the study area consists essentially of an old migmatized and granitized base with some birrimian intrusions. The geology can be subdivided in Voltaian, Birrimian and Precambrian units as described by Adu[53]. The Voltaian is represented by sandstones and shale locally confined along the White Volta River. The Birrimian is composed of metamorphosed sediments and volcanic rocks, although arenaceous conglomerates and argillaceous rocks are also found. The Precambrian in the area is dominated by granitic rocks described as compound gneisses in the Navrongo. Four main soil classes are observed. Soils derived from granites consist mainly of sandy soil in the series of Tanchera and Bongo associations. The topsoil is loose, porous, coarse textured and easy to cultivate; however, it is also easily eroded and poorly supplied with nutrients and of low capacity to retain moisture. They are suitable for the cultivation of guinea corn, millet, groundnuts and beans. Over Birrimian rocks the predominant soil association is the Bianya series. The topsoil is light grey silty or fine sandy clay colluvium, overlying quartz gravel and stones or weathering rock. It frequently supports Acacia tree species with canopies that poorly cover the surface. The Voltaian rocks develop mainly Kintampo soil series which is associated with lithosols often accompanied by bare rock outcrops found along the Pendjari and the White Volta River. On these soils vegetative cover is poor and consists only of short grasses and shrubs. Soils derived from Quaternary and Tertiary rocks consist of Siare-Bonabi-Dagare series and occur extensively along the alluvial tracts of the major tributary rivers of the Kompienga and the Volta Rivers. They are deep to very deep fertile soils well suited for mechanized cultivation of rice, cotton, sugarcane and vegetables. They usually support rich woodland to gallery forest vegetative layers.

The vegetation in the study area has been classified as "transition zone between wet and dry savannah", tree savannah, savannah woodland, or simply savannah. The original vegetation composed mainly of deciduous trees in grassland, is heavily influenced by human agricultural and deforestation activities including livestock overgrazing and periodic bush fires. Moreover, this savannah is also prone to erratic climatic conditions dominated by high inter-annual rainfall variability. The natural vegetation is composed basically of woodlands on varying soil conditions. Common tree species are *Anogeissus leiocarpus,* (Loa, local in Mapprussi language)*, Vitellaria paradoxa* (Sungu) and *Parkia biglobosa* (Dawa-dawa) *Acacia* occur frequently and are usually found on heavy clay soils associated with old river alluvium, piedmont slopes and eroded sites. Riverine woodland tenuously fringes the *White* and *Red Volta*, the *Sissili* and a few of the minor streams. Around populated areas of Navrongo and Bolgatanga, tree density is low as a result of land degradation and deforestation for new farms, fuel wood, building and other purposes. Main cultivated crops are cotton, tobacco, tomato, black pepper, sweet potato, millet, guinea corn, maize, cowpeas, bambara beans, cassava and yam. The

agricultural landscape, composed of compound and bush farms, is an agro-forestry park with few indigenous tree species preserved for their economic value. Most common tree species include *Vitellaria paradoxa, Parkia biglobosa, Acacia albida, Anogeissus leiocarpus, Adansonia digitata* (baobab), *Tamarindus indica, Mangifera indica* and *Ceiba pentandra*.

4. SATELLITE IMAGES

SEBAL[NM] has been used to derive maps of the sensible and latent heat fluxes as well as root zone soil moisture from four images: two Landsat and two MODIS (Table 2). The October 2002 and March 2003 images represent the hydrological conditions, respectively, at the start and at the end of the dry season. The March 2003 Landsat and MODIS images have been taken at the same date at approximately the same time of the morning. The October images differ by four days due to the fact that the MODIS image of October 30, 2002, was corrupted.

The use of SEBAL[NM] on Landsat and MODIS images has been described before in the SPIE proceedings[24, 25].

Table 2.   LandSat and MODIS images used in this study for SEBAL applications.

Satellite	Area	Path/Row of Landsat	Date
LandSat7	Bolgatanga	194-52/53	10/30/2002
LandSat7	Bolgatanga	194-53	03/07/2003
MODIS	Bolgatanga	NA	10/26/2002
MODIS	Bolgatanga	NA	03/07/2003

5. RESULTS AND DISCUSSION

Figure 2 presents the MODIS and Landsat images of October 26 and 30, 2002, respectively, that are used for the SEBAL[NM] analysis at the end of the rainy season. The Landsat image of October 30 is a composite of two images (Path 194, Rows 52 and 53). On March 7, 2003, at the end of the dry season only the southern Landsat image (Path 194, Row 53) was used. The MODIS image of October 26 was used since the October 30 image was corrupted with severe striping.

5.1 Maps derived from Landsat images

Figure 3 presents the maps of ET, sensible heat flux, and soil moisture (degree of saturation) at the end of the dry season on March 7, 2003. There is some cloud contamination in the upper NW corner of the image. The ET values over the area are very small (zero or close to zero) over most of the area and net radiation is largely converted into sensible heat flux. Therefore, turbulent transport by buoyancy forces will be common in this period. Soil moisture is low throughout the area with the exception of the irrigated area in the NW corner of the image below Tono dam and all along the valley of the White Volta river. The White Volta river is particularly well delineated in the soil moisture map.

Figure 4 presents the maps of ET, sensible heat flux, and soil moisture at the end of the rainy season on October 30, 2002. The lower half of Figure 4 represents the area pictured in Figure 3. As expected, the ET rates are much higher than at the end of the dry season and vary mostly between 2-4 mm/day in the southern part of the map. The sensible heat fluxes are considerably lower since much of the net radiation is used for evapotranspiration, so that atmospheric turbulence will be less than at the end of the dry season.

Figure 5 presents the maps of ET, sensible heat flux, and soil moisture at the end of the dry season on March 7, 2003, around Tono dam. The size of this map is about 10 by 15 km. These maps demonstrate the high spatial resolution of maps derived from Landsat images. The irrigated rice fields as well as the wetlands along the river can be identified.

5.2 Maps derived from MODIS images

Figure 6 presents the maps of ET, sensible heat flux, and soil moisture at the end of the dry season on March 7, 2003, derived from a MODIS image. The spatial resolution of this map is 1000 by 1000 m and, therefore, much of the fine details found on the Landsat ET map have disappeared. For example, the rather narrow valley of the White Volta river

visible in the Landsat ET map (see Fig. 3) can hardly be recognized. Overall, the Landsat and MODIS ET maps appear very similar. The histograms of the Landsat and MODIS ET maps also show good agreement (Figure 7), although the mean ET of 0.48 mm/day from the MODIS ET map is double the mean ET of 0.24 mm/day from the Landsat ET map. However, both numbers are rather small and thus concur the ET is very low. In previous work we have shown that the relative error of SEBAL[NM] ET difference estimates between Landsat and MODIS ET maps decreases from more than 100% at very low ETs like 0.3 mm/day to about 10% at high ETs like 6-8 mm/day[25]. The standard deviation of ET in the MODIS ET map is lower than the standard deviation in the Landsat ET map due to the much larger pixel size of the MODIS image.

The ET histograms from the ET maps derived from Landsat and MODIS on October 30 and 26, 2002, respectively, do not agree at all (Figure 8). The ET values from the MODIS ET map are higher and show a bimodal distribution. In addition, the average ET values also differ by more than 2 mm/day as do the standard deviations. The ET standard deviation from the MODIS ET map is more than twice the standard deviation from the Landsat ET map. These anomalies have not been caused by precipitation since very little rain was observed during the period October 18-30, 2002. Careful inspection of the MODIS image revealed a thin transparent cloud cover over most of the image. These thin clouds were sufficient to lower the apparent surface temperature of many dry pixels which in the SEBAL[NM] algorithm results in an erroneous higher ET estimate. Therefore, it is concluded that the MODIS ET map of October 26, 2002, is not correct. Nevertheless this erroneous map provides an instructive example, illustrating that the SEBAL approach only works on clear days when few or no clouds are present. Particularly in the tropics, care should be taken to select images without thin transparent clouds.

6. SUMMARY

In this case study of the White Volta Basin in Ghana it is demonstrated that maps of evapotranspiration, sensible heat flux, and root zone soil moisture can be obtained using SEBAL[NM] using few or no ground measurements provided a Landsat or MODIS optical image is available. This case study joins an abundance of similar studies reported in the literature in providing strong evidence that the SEBAL approach is a powerful tool for the characterization of surface energy balances anywhere in the world using readily available satellite images. However, great care is needed to select images that are free of thin transparent cloud cover since clouds cause erroneously high ET and soil moisture estimates.

ACKNOWLEDGEMENT

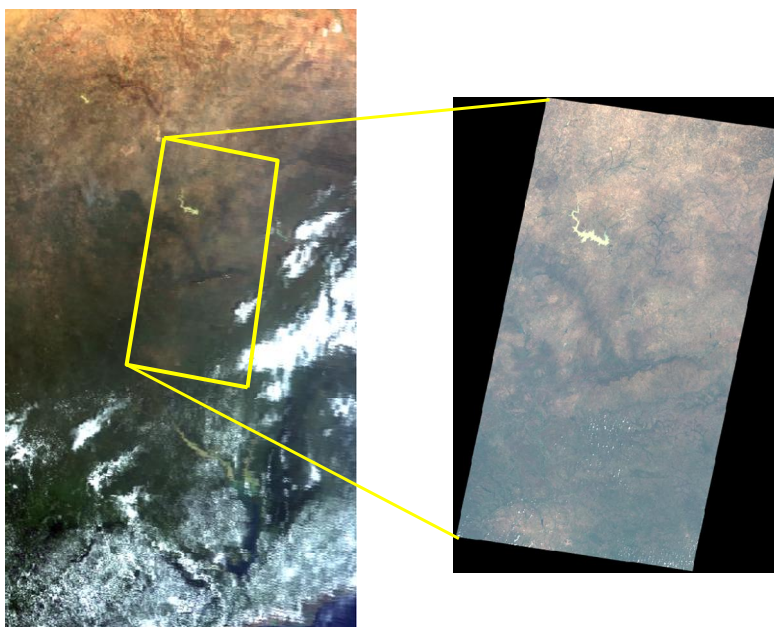**MODIS image on Oct. 26 2002   Landsat image on Oct. 30 2002**

Figure 2. MODIS and Landsat images at the end of the rainy season. The Landsat image is composed of two images (Path 194, Rows 52 and 53). At the end of the dry season (March 7, 2003) only the southern image was used (Path 194, Row 53).

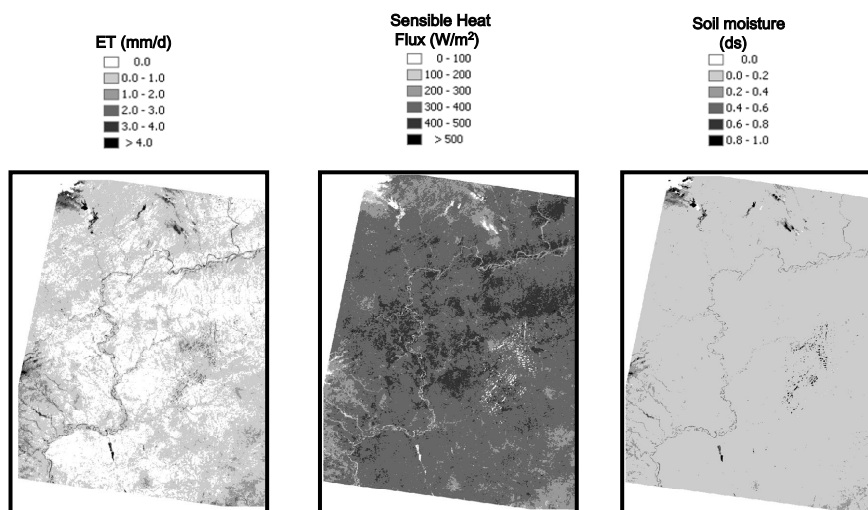## Landsat SEBAL^{NM} results on March 07 2003

Figure 3. Maps of ET, sensible heat flux, and soil moisture (degree of saturation) at the end of the dry season (March 7, 2003) derived from Landsat image. There is some contamination by clouds in the upper NW corner of the image.

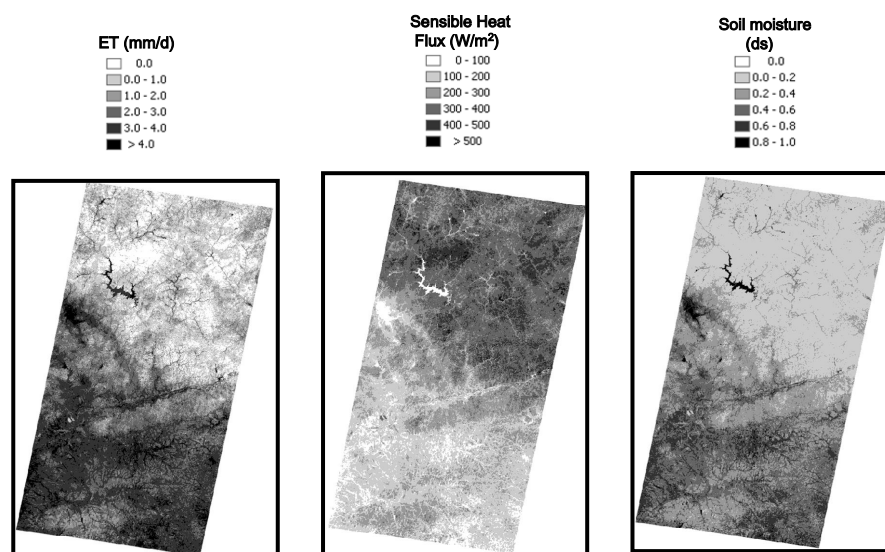## Landsat SEBAL^NM results on Oct. 30 2002

Figure 4. Maps of ET, sensible heat flux, and soil moisture (degree of saturation) at the end of the rainy season (October 30, 2002) derived from Landsat image. The scale of these maps is different from Figure 3 since the maps cover two Landsat images. The area of Figure 3 is the lower half of this figure.
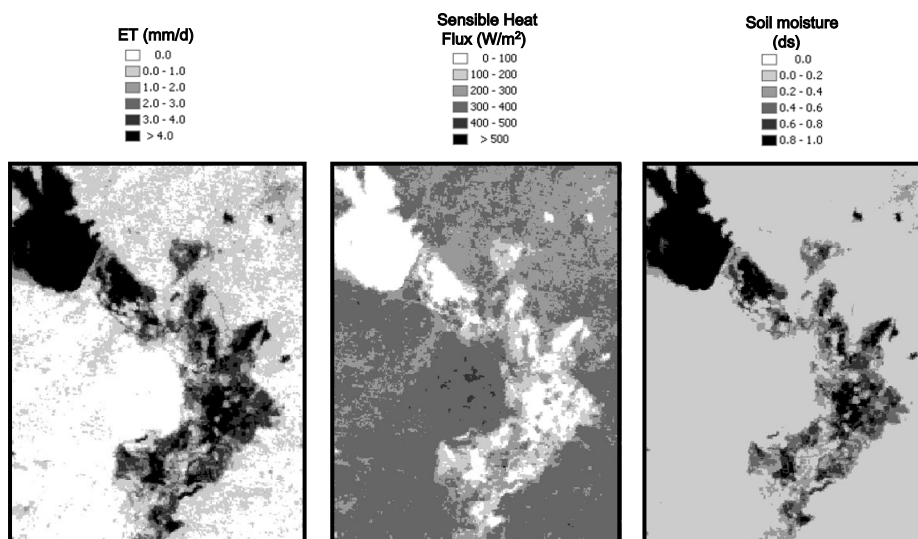
Landsat SEBAL^NM results on March 07 2003

Figure 5. Maps of ET, sensible heat flux, and soil moisture (degree of saturation) around Tono dam at the end of the dry season (March 7, 2003) derived from Landsat image. The size of these maps is approximately 10 by 15 km. Spatial resolution of heat fluxes and soil moisture maps is 30 m.

March 7, 2003
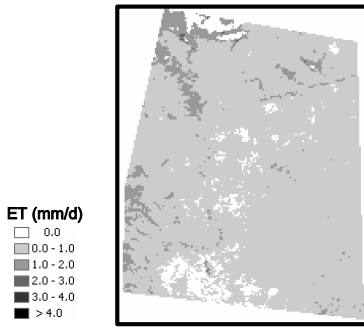
Landsat histogram

MODIS histogram

Figure 6. Map of ET at the end of the dry season (March 7, 2003) derived from MODIS image. The spatial resolution of this map is 1000 by 1000 m.
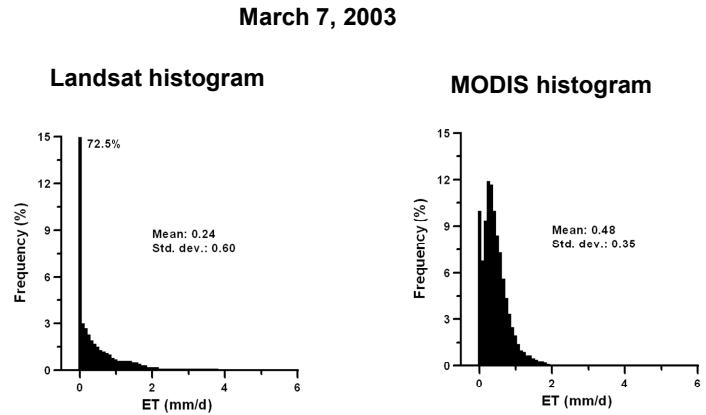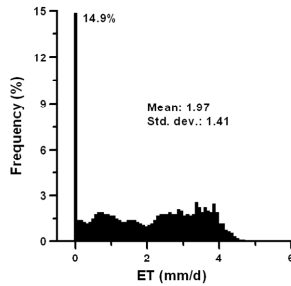
Figure 7. ET histograms of Landsat and MODIS ET maps on March 7, 2003.

October 30, 2002
Landsat histogram
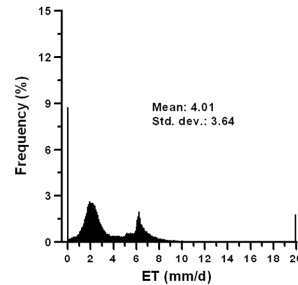

October 26, 2002
MODIS histogram

Figure 8. ET histograms of Landsat and MODIS ET maps on, respectively, October 30 and 26, 2002. The peak of high ET values in the MODIS histogram are caused by thin transparent clouds covering the image. Therefore, this MODIS ET map is not reliable.

REFERENCES

1.   Mason, G.L. *Short-term operational forecasts of trafficability (SOFT).* in *2000 Spring Simulation Interoperability Workshop.* 2000. Orlando, FL.

2.   Miller, T.W., J.M.H. Hendrickx, and B. Borchers, *Radar Detection of Buried Landmines in Field Soils.* Vadose Zone J, 2004. **3**: p. 1116-1127.

3.   Miller, T.W., et al., *Effect of soil moisture on land mine detection using ground penetrating radar.* Proc. International Society for Optical Engineering, SPIE, 2002. **4742**: p. 281-290.

4.   Rhebergen, J.B., et al., *Prediction of soil effects on GPR signatures.* Proc. International Society for Optical Engineering, SPIE, 2004. **5415**: p. 705-715.

5.   Van Dam, R.L., B. Borchers, and J.M.H. Hendrickx, *Soil effects on thermal signatures of buried nonmetallic landmines.* Proc. International Society for Optical Engineering, SPIE, 2003. **5089**: p. 1210-1218.

6. Šimůnek, J., J.M.H. Hendrickx, and B. Borchers, *Modeling transient temperature distributions around landmines in homogeneous bare soils.* Proc. International Society for Optical Engineering, SPIE, 2001. **4394**: p. 387-397.

7. Rhebergen, J.B., et al., *Soil moisture distribution around land mines and the effect on relative permittivity.* Proc. International Society for Optical Engineering, SPIE, 2002. **4742**: p. 269-280.

8. Hong, S.-H., et al., *Land mine detection in bare soils using thermal infrared sensors.* Proc. International Society for Optical Engineering, SPIE, 2002. **4742**: p. 43-50.

9. Hong, S.-H., et al., *Impact of soil water content on landmine detection using radar and thermal infrared sensors.* Proc. International Society for Optical Engineering, SPIE, 2001. **4394**: p. 409-416.

10. Hendrickx, J.M.H., B.S. Das, and B. Borchers, *Modeling distributions of water and dielectric constants around land mines in homogeneous soils.* Proc. International Society for Optical Engineering, SPIE, 1999. **3710**(2): p. 728-738.

11. Hendrickx, J.M.H., et al., *Spatial variability of dielectric properties in field foils.* Proc. International Society for Optical Engineering, SPIE, 2001. **4394**: p. 398-408.

12. Das, B.S., J.M.H. Hendrickx, and B. Borchers, *Modeling transient water distributions around landmines in bare soils.* Soil Science, 2001. **166**(3): p. 163-173.

13. Van Dam, R.L., B. Borchers, and J.M.H. Hendrickx, *Strength of landmine signatures under different soil conditions: implications for sensor fusion.* International Journal of Systems Science, 2005. **36**(9): p. 573-588 DOI: 10.1080/00207720500147800.

14. Niedzialek, J.M. and F.L. Ogden, *Runoff production in the upper Rio Chagres catchment, Panama*, in *The Rio Chagres: A multidisciplinary profile of a tropical watershed*, R.S. Harmon, Editor. 2005, Springer: Dordrecht, The Netherlands. p. 149-168.

15. Dingman, S.L., *Physical Hydrology*. 2002, Upper Saddle River, New Jersey 07458: Prentice Hall. 646.

16. Calvo Gobbette, L.E., F.L. Ogden, and J.M.H. Hendrickx, *Infiltration in the Upper Rio Chagres basin. The soil conservation service "curve numbers"*, in *The Rio Chagres: A multidisciplinary profile of a tropical watershed*, R.S. Harmon, Editor. 2005, Kluwer Academic Publishers: Dordrecht, The Netherlands.

17. Senarath, S.U.S., et al., *On the calibration and verification of distributed, physically-based, continuouous, Hortonian hydrologic models.* Water Resour. Res., 2000. **36**(6): p. 1495-1510.

18. Ogden, F.L., et al., *Hydrologic analysis of the Fort Collins, Colorado, flash flood of 1997.* J. Hydrology, 2000. **228**: p. 82-100.

19. Downer, C.W., et al., *Theory, development, and applicability of the surface water hydrologic model CASC2D.* Hydrological Processes, 2002. **16**(2): p. 255-275.

20. Downer, C.W. and F.L. Ogden, *Users Manual: Gridded Surface/Subsurface Hydrologic Analysis*, in *Engineering Research and Development Center Technical Report*. 2003, U.S. Army Corps of Engineers.

21. Scott, C.A., W.G.M. Bastiaanssen, and M.-u.-D. Ahmad, *Mapping Root Zone Soil Moisture Using Remotely Sensed Optical Imagery.* J. Irrig. and Drain. Engrg., 2003. **129**(5): p. 326-335.

22. Campbell, G.S. and J.M. Norman, *An introduction to environmental biophysics. Second Edition*. 1998, New York, NY: Springer. 286.

23. Brutsaert, W., *Evaporation into the atmosphere*. 1982, Dordrecht, The Netherlands: D. Reidel Pub. Co. 307.

24. Hendrickx, J.M.H. and S.-h. Hong, *Mapping sensible and latent heat fluxes in arid areas using optical imagery.* Proc. International Society for Optical Engineering, SPIE, 2005. **5811**: p. 138-146.

25. Hong, S.-h., J.M.H. Hendrickx, and B. Borchers, *Effect of scaling transfer between evapotranspiration maps derived from LandSat 7 and MODIS images.* Proc. International Society for Optical Engineering, SPIE, 2005. **5811**: p. 147-158.

26. Wang, J., et al., *Aggregation of land surface parameters in the oasis-desert systems of Northwest China.* Hydr. Processes, 1998. **12**: p. 2133-2147.

27. Trezza, R., *Evapotranspiration using a satellite-based surface energy balance with standardized ground control*. 2002, Utah State University: Logan, Utah.

28. Tasumi, M., *Progress in operational estimation of regional evapotranspiration using satellite imagery*. 2003, University of Idaho: Moscow, Idaho.

29. Roerink, G.J., et al., *Relating crop water consumption to irrigation water supply by remote sensing.* Water Resources Management, 1997. **11**: p. 445-465.

30.   Pelgrum, H. and W.B.M. Bastiaanssen, *An intercomparison of techniques to determine the area-averaged latent heat flux from individual in situ observations: a remote sensing approach using the European Field Experiment in a Desertification-Threatened Area data.* Water Res. Res., 1996. **32**: p. 2775-2786.

31.   Morse, A., et al., *Application of the SEBAL methodology for estimating consumptive use of water and streamflow depletion in the Bear river basin of Idaho through remote sensing. Final Report, Phase I.* 2000, Department of Water Resources and University of Idaho. p. 107.

32.   Bastiaanssen, W.G.M., et al., *A remote sensing surface energy balance algorithm for land (SEBAL). Part 2: Validation.* Journal of Hydrology, 1998. **212-213**: p. 213-229.

33.   Bastiaanssen, W.G.M., et al., *A remote sensing surface energy balance algorithm for land (SEBAL): 1. Formulation.* Journal of Hydrology, 1998. **212-213**: p. 198-212.

34.   Bastiaanssen, W.G.M., *SEBAL-based sensible and latent heat fluxes in the Irrigated Gediz Basin, Turkey.* J. of Hydrology, 2000. **229**: p. 87-100.

35.   Bastiaanssen, W.G.M., et al., *SEBAL model with remotely sensed data to improve water-resources management under actual field conditions.* J. Irrig. and Drain. Engrg., ASCE, 2005. **131**(1): p. 85-93.

36.   Bastiaanssen, W.G.M., M.D. Ahmad, and Y. Chemin, *Satellite surveillance of evaporative depletion across the Indus Basin.* Water Resour. Res., 2002. **38**: p. 1273-1281.

37.   Van de Hurk, B.J.J.M., W.G.M. Bastiaanssen, H. Pelgrum, and E. van Meijgaard, *A new methodology for assimilation of initial soil moisture fields in weather prediction models using Meteosat and NOAA data.* Journal of Applied Meteorology, 1997. **36**: p. 1271-1283.

38.   Iqbal, M., *An introduction to solar radiation*. 1983, Toronto: Academic Press.

39.   Brutsaert, W., A.Y. Hsu, and T.J. Schmugge, *Parameterization of surface heat fluxes above a forest with satellite thermal sensing and boundary layer soundings.* Jour. Appl. Meteorol., 1993. **32**: p. 909-917.

40.   Kustas, W.P. and J.M. Norman, *Use of remote sensing for evapotranspiration monitoring over land surfaces.* Hydrol. Sci. Jour., 1996. **41**: p. 495-515.

41.   Franks, S.W. and K.J. Beven, *Estimation of evapotranspiration at the landscape scale: a fuzzy disaggregation approach.* Water Resour. Res., 1997. **33**: p. 2929-2938.

42.   Farah, H.O., *Estimation of regional evaporation under different weather conditions from satellite and meteorological data. A case study in the Naivasha Basin, Kenya*, in *Soil Physics, Agrohydrology and Groundwater Management*. 2001, Wageningen Univ.: Wageningen. p. 170.

43.   Rosema, A., *Comparison of meteosat-based rainfall and evapotranspiration mapping of Sahel region.* Remote Sens. Env., 1990. **46**: p. 27-44.

44.   Kalman, J.D. and D.L.B. Jupp, *Estimating evaporation from pasture using infrared thermography: evaluation of a one-layer resistance model.* Agr. Forest Meteorol., 1990. **51**: p. 223-246.

45.   Hall, F.G., et al., *Satellite remote sensing of the surface energy balance: success, failures and unresolved issues in FIFE.* Jour. Geophys. Res., 1992. **97**: p. 19061-19090.

46.   Huette, A.R., *Soil-adjusted vegetation index (SAVI).* Remote Sens. Env., 1988. **25**: p. 89-105.

47.   Ahmad, M.-u.-D. and W.G.M. Bastiaanssen, *Retrieving soil moisture storage in the unsaturated zone using satellite imagery and bi-annual phreatic surface fluctuations.* Irrigation and Drainage Systems, 2003. **17**(3): p. 141-161 doi:10.1023/A:1025101217521.

48.   Fleming, K., J.M.H. Hendrickx, and S.-h. Hong, *Regional mapping of root zone soil moisture using optical satellite imagery.* Proc. International Society for Optical Engineering, SPIE, 2005. **5811**: p. 159-170.

49.   Amisigo, B.A., *Modelling riverflow in the Volta Basin of West Africa: a data-driven framework.* Ecology and Development Series. Vol. 34. 2005, Bonn, Germany: Center for Development Research, University of Bonn. 183.

50.   Compaore, H., *The impact of savannah vegetation on the spatial and temporal variation of the actual evapotranspiration in the Volta Basin, Navrongo, Upper-East Ghana.* Ecology and Development Series. Vol. 36. 2006, Bonn, Germany: Center for Development Research, University of Bonn. 153.

51.   Koné, N., *Contribution à l'étude du fonctionnement des écosystèmes naturels en zone, soudano sahélienne (Cas du Burkina Faso). Approche de la dynamique de la sécheresse par télédétection*. 1992, Univ. Toulouse, ICIV: Toulouse, France. p. 207.

52.   Muller, E., *Etude de la végétation de la région de Kongoussi (Burkina Faso) à partir données MSS-Landsat du 12 Nov. 1972 et du 6 Nov. 1975*, in *Rapport DESS, CETEL-GDTA*. 1985. p. 86.

53.   Adu, S.V., *Soils of the Navrongo-Bawku area, Upper Region, Ghana*. 1969, Soil Research Institute: Kumasi. p. 96.